Mathematical Modeling of Pulsing Flow in Large Trickle Beds

A crossflow model for pulsing flow in a trickle bed of large cross section is presented. The trickle bed is idealized as being made up of pulses and the trickling flow region surrounding these pulses. Assuming the macroscopic gas flow around the pulses to be irrotational and the pulses to contain only liquid, the model equations are derived. An analysis of the model and comparison with the experimental results of Christensen (1986) reveals that the irrotational flow model underestimates the pulse velocity for realistic pulse shapes. This can be attributed to the underestimation by the model of the drag exerted by the trickling region on the pulses. By dropping the irrotational flow assumption and viewing the model as semiempirical, a single parameter characterizing the magnitude of this drag is estimated from the pulse velocity data. When this estimated value for this parameter is employed, the model predicts the average pressure gradient data reasonably well.

S. Sundaresan
Department of Chemical Engineering
Princeton University
Princeton, NJ 08544

Introduction

Trickle beds in which a gas and a liquid flow concurrently over a solid packing are widely used in the petroleum and chemical industries. Numerous studies of hydrodynamics, mass transfer, and reactions in these systems have been published and these are summarized by Satterfield (1975), Gianetto et al. (1978), Hoffmann (1978), Shah (1979), Koros (1981), and Herskowitz and Smith (1983). A variety of flow regimes are encountered in trickle beds, the two most commonly encountered being trickle flow, which is obtained at low liquid and gas flow rates, and pulsing flow at high liquid and gas flow rates. A number of industrial reactors operate near the trickling-to-pulsing transition (Satterfield, 1975). An understanding of the conditions at which transition from one regime to another occurs, as well as of the nature of two-phase flow in each of these regimes, is of fundamental importance in the design and scale-up of these reactors.

Pulsing flow, obtained at high gas and liquid flow rates, is characterized by large fluctuations in pressure drop and liquid holdup. Most of the experimental work on pulsing reported in the literature has been performed in small-diameter (<0.1 m) cylindrical columns. These studies led to a visualization of pulsing flow as the alternating passage of liquid-rich and gas-rich regions down the column (Weekman and Myers, 1964; Beimesch and Kessler, 1971; Blok and Drinkenburg, 1982). Such a visualization has been used by Dimenstein and Ng (1986) to develop a mathematical model for pulsing flow. There exists, however, a fundamental difficulty in extrapolating the visualization of pulsing from the small-diameter laboratory column to large-diameter industrial columns. In every laboratory study, the liquid-rich region in the pulsing flow apparently filled most of the column cross section, suggesting that the size and shape of the liquid-rich region in the pulsing flow were limited by the column diameter. It is difficult to believe that this would happen in large-diameter industrial columns.

In an effort to develop a conceptual model for the pulsing flow in packed columns with large cross-sectional areas, we recently studied (Christensen et al., 1986) the characteristics of pulsing in a packed column of rectangular cross section to obtain an effectively two-dimensional flow behavior. The most striking observation was that the pulses (i.e., slugs of liquid-rich regions) did not always span the column cross section, as they did in small-diameter columns. Pulses not spanning the column cross section were curved concavely downward. As the flow rates were increased, the pulses became wider and flatter. The pressure drops observed in this column were considerably lower than the predictions by literature correlations (Sato et al., 1973; Midoux et al., 1976; Tosun, 1984) that were obtained from experiments in small-diameter columns, indicating that large differences exist between the nature of pulsing flow in small-diameter columns and columns of large cross section. Average liquid holdups measured in the column of rectangular cross section over a wide range of conditions in the pulsing regime agreed well with the predictions of Sato et al. and of Midoux et al., indicating that

the liquid holdup is approximately independent of column cross-sectional area. The velocity and frequency of pulses measured in the column of rectangular cross section were consistently lower than those reported in the literature (Rao and Drinkenburg, 1983) for equivalent throughputs in small-diameter columns. The lower pressure drops and pulse velocities observed in the column of rectangular cross section were interpreted as being due to the bypassing of gas around the edge of the pulses (Christensen et al., 1986).

A mathematical model that captures the essential characteristics of the two-phase flow in the pulsing regime at least in a qualitatively correct fashion is indispensible for design and scale-up of processes operating in this regime. It is readily apparent that any reasonable model should take into consideration the following issues. For a given set of throughput of gas and liquid in the pulsing regime:

1. What are the conditions (e.g., average liquid holdup) present in the pulses and in the relatively gas-rich region surrounding these pulses?
2. What fraction of the bed volume is occupied by these pulses?
3. How fast are these pulses moving down the column?
4. At what rate are these pulses exchanging matter (in the liquid as well as gas phase) with the gas-rich region surrounding them?

This is by no means a complete list of questions; rather, it is a sample of the important ones. The state of mathematical modeling has largely remained primitive until recently. A few studies have attempted to incorporate the essential characteristics of the flow fields (Lerou et al., 1980; Dimenstein and Ng, 1986). However, these analyses are valid only for small-diameter packed columns. There does not exist even a single mathematical model that incorporates in a qualitatively correct fashion the essential characteristics of pulsing flow in large-diameter packed columns, and our ultimate objective is to develop such a model. Before such a mathematical model can be developed, it is essential that we obtain an (at least qualitative) understanding of the two-phase flow fields in a pulse and in the gas-rich region surrounding this pulse. Our recent experiments (Christensen et al., 1986) have revealed a striking conceptual similarity between pulsing flow in packed columns and the motion of bubbles in fluidized beds. The possible existence of such a similarity was speculated on by McGovern (1982).

In fluidized beds, for gas throughputs above that for minimum fluidization, one obtains a bubbling flow in beds of large cross section. These bubbles are small compared to the diameter of the bed. If the gas is distributed uniformly at the inlet, these bubbles are usually located randomly across the bed cross section. These bubbles have a sharp leading edge and a trailing wake. However, if the bed diameter is small, the size of the bubbles becomes limited by the bed diameter and one obtains a slugging fluidized bed. The slugs of gas moving up the bed still maintain a sharp leading edge and a diffuse wake (Davidson and Harrison, 1971).

Conceptually, the pulses (i.e., slugs of liquid-rich region) in a trickle bed are not very different from the bubbles in a fluidized bed (although trickle beds contain an additional phase). The pulses have a sharp front with a diffuse wake. If the bed diameter is large and the distribution (of gas and liquid) at the inlet is uniform, these pulses are small compared to the bed diameter and are randomly located across the bed cross section. However, if the bed diameter is small, these pulses become limited by the bed diameter, while still maintaining a sharp leading front and diffuse wake.

In fluidized beds, the conditions (e.g., void fraction) in the emulsion phase (far away from the bubbles) are close to those corresponding to minimum fluidization. Experimental evidence from studies on pulsing flow suggests that the flow pattern in the gas-rich region is predominantly trickling, i.e., liquid trickling over the solid packing with a continuous gas phase. Further, scattered experimental evidence suggests that the conditions in this trickling region (far away from the pulses) are close to those corresponding to the onset of pulsing. Strictly speaking, this last statement is only a conjecture, although plausible. The type of experiments that would verify the validity of this conjecture is, however, not obvious at the present time.

The approach to analyzing pulse motion in trickle beds described below is an adaptation of the analysis of bubble motion in fluidized beds by Davidson (1961) and later refinements summarized by Jackson (1971), with appropriate modifications to render the analysis suitable for trickle beds.

A Model for Pulse Motion

For the purpose of analysis, one can divide the trickle bed operating in the pulsing regime into three regions: the pulses, the wake region behind these pulses, and the trickling flow region surrounding the pulses and the wakes. The pulse itself can be approximately viewed as a liquid-continuous region with entrained gas bubbles (Blok et al., 1983; Dimenstein and Ng, 1986). The trickling region may be idealized as being at conditions corresponding to the onset of pulsing. The liquid holdup in the pulses is substantially higher than that in the trickling region. The wake region, which is difficult to model, represents a gradual transition from the higher liquid holdup condition present in a pulse to the lower liquid holdup level of the trickling region. It is exceedingly complex and probably unrealistic to attempt (with the current level of understanding of the hydrodynamics in the pulsing regime) to model the two-phase flow fields in their entirety, retaining all the three regions described above. Hence, in order to render the problem tractable we make several simplifying assumptions as discussed below.

We shall neglect the wake region completely so that we have to treat only the pulse and the surrounding trickling region. Although this is a drastic simplification of the problem, it is a necessary one at the present time in order to formulate any kind of mathematical model for such a complex system.

We also assume that the pulse is made up of only liquid. Even though the pulse does contain entrained gas bubbles, treating the pulse as a pocket of liquid is a reasonably good first approximation as the volume fraction of gas bubbles inside the pulse is usually small.

Let us consider a trickle bed of uniform porosity ϵ operating in the pulsing regime with gas and liquid throughputs of G and L ($kg/m^2 \cdot s$), respectively. We assume, for simplicity, that the two phases are incompressible. We also assume that there are no inherent maldistributions in the packing or the gas and liquid feed at the top of the column so that the pulses are randomly distributed along the column cross section when the pulse size is small compared to the column cross section. In our analysis, we shall consider a "three-dimensional" column, by which we refer to a long cylindrical packed column of very large diameter, as

well as a "two-dimensional" column, by which we refer to a long packed column of very large width and finite thickness (so that the flow patterns are essentially two-dimensional in nature).

From a macroscopic viewpoint, it appears reasonable to idealize the flow pattern by a simple crossflow model as shown schematically in Figure 1. Accordingly, a fraction f_p of the column cross section at any height is occupied by the pulses, while in the remainder of the region we have a trickling flow. The pulses contain only liquid and this liquid is moving down the column at an average interstitial velocity of $u^{\circ}_{\ell p}$. The average interstitial velocities of the gas and liquid in the trickling region are u^{∞}_{gt} and $u^{\infty}_{\ell t}$, respectively and the liquid holdup there is β_t. A macroscopic description of this type is useful when analyzing performance characteristics such as dispersion in the liquid phase, mass transfer, and so on. For such a model,

$$G = \epsilon\rho_g(1 - \beta_t)(1 - f_p)u^{\infty}_{gt} \tag{1}$$

$$L = \epsilon\rho_\ell[u^{\circ}_{\ell p}f_p + (1 - f_p)\beta_t u^{\infty}_{\ell t}]. \tag{2}$$

Let us first consider the trickling region. In general, one has to consider flow nonuniformities such as rivulets in modeling trickling flow. However, it appears that these rivulets are broken apart by increasing gas-liquid interaction as one approaches conditions corresponding to the onset of pulsing (Christensen et al., 1986). Therefore, for the purpose of our analysis, in which we shall postulate that the conditions in the trickling region are those corresponding to the onset of pulsing, we can assume that the liquid in the trickling region flows in the form of a film over a solid packing with the gas flowing in the interstices. We also assume that the liquid wets the solid completely. It is then straightforward to show that the flow of gas and liquid in the trickling region under steady state conditions is described by the following volume-averaged continuity and approximate momentum balance equations.

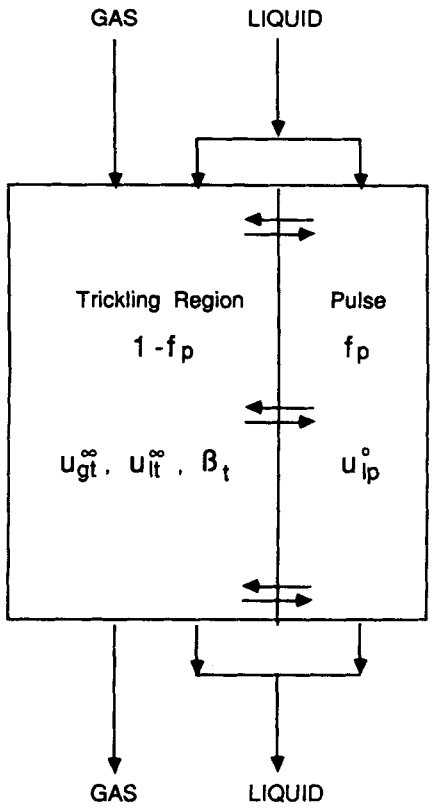

Figure 1. Crossflow model representation of pulsing flow in trickle beds of large cross section.

f_p, fraction of bed occupied by pulses
u^{∞}_{gt}, average velocity of gas in trickling region
$u^{\infty}_{\ell t}$, average velocity of liquid in trickling region
$u^{\circ}_{\ell p}$, average velocity of pulse in trickling region
β_t, liquid holdup

$$\nabla \cdot (\beta_t \underline{u}_{\ell t}) = \nabla \cdot [(1 - \beta_t)\underline{u}_{gt}] = 0 \tag{3}$$

$$\epsilon\rho_g(1 - \beta_t)\underline{g} - \epsilon(1 - \beta_t)\nabla p_{gt} + \underline{F}^t_{g\ell} = \underline{0} \tag{4}$$

$$\epsilon\rho_\ell\beta_t\underline{g} - \epsilon\beta_t\nabla p_{\ell t} + \underline{F}^t_{\ell g} + \underline{F}^t_{\ell s} = \underline{0} \tag{5}$$

$$p_{gt} - p_{\ell t} + 2\sigma_\ell H_t = 0 \tag{6}$$

$$\underline{F}^t_{g\ell} + \underline{F}^t_{\ell g} + \underline{M}^t = \underline{0} \tag{7}$$

The macroscopic inertial terms, and the Reynolds and deviatorial stress tensors have been neglected in the above momentum balance equations as it can easily be argued that these terms are unlikely to be significant. In order to use the above equations we must first postulate constitutive relations for the various interaction forces and the average curvature. Although semiempirical forms for some of these terms have been suggested in the literature (for example, by Saéz and Carbonell, 1985), we shall use rather simple constitutive relationships in our analysis. This seems adequate at the present time as our goal is to sort out in a qualitative fashion the various features of pulsing flow known from experiments to identify those features that are important in any rational description of pulsing.

Very little is known at the present time about the interaction force arising from the local fluctuations in the curvature, $\underline{M}^t$, and to the best of our knowledge the importance of this term has not yet been proved in any systematic manner. We shall neglect this term in our analysis. We postulate that the average curvature H_t is only a function of β_t and the physical properties of the fluids and packing (e.g., particle size). Thus, a spatial variation of H_t in the trickling region arises only if the liquid holdup is a function of position.

The interaction force $\underline{F}^t_{g\ell}$ would primarily depend on β_t, $\underline{u}_{gt}$ and $\underline{u}_{\ell t}$, and to a lesser degree on the gradients in these quantities. The simplest form for $\underline{F}^t_{g\ell}$ would be: $\underline{F}^t_{g\ell} = -a^t(\underline{u}_{gt} - \underline{u}_{\ell t})$, where a^t is a proportionality constant. In situations of practical interest $|\underline{u}_{gt}| \gg |\underline{u}_{\ell t}|$, and hence we can approximate the above constitutive relation further as

$$\underline{F}^t_{g\ell} = -a^t\underline{u}_{gt}. \tag{8}$$

An approximate expression for a^t can be written in terms of a modified Ergun equation (Specchia and Baldi, 1977) as

$$a^t = a_{1t} + a_{2t}|\underline{u}_{gt}| \quad \text{where} \tag{9}$$

$$a_{1t} = k_{1t}[1 - \epsilon(1 - \beta_t)]^2\mu_g/\epsilon(1 - \beta_t)d_e^2 \tag{10}$$

$$a_{2t} = k_{2t}[1 - \epsilon(1 - \beta_t)]\rho_g/d_e \tag{11}$$

Here k_{1t} and k_{2t} are coefficients in the modified Ergun equation, to be determined from experimental data on pressure drop for gas flow through a wetted packing (Specchia and Baldi). The above equation assumes that the only manner in which the liquid phase enters the momentum equation for the gas phase is by a decrease in the cross-sectional area available for gas flow caused by the presence of liquid. Although the above constitutive relation is not strictly complete, it does indeed represent a major fraction of the actual gas-liquid interaction (Specchia and Baldi, 1977; Christensen et al., 1986). We make one additional simplification by rewriting Eq. 9 as

$$a^t \simeq a_{1t} + a_{2t}u_{gt}^{\infty}. \tag{12}$$

This is a reasonable assumption, as u_{gt}^{∞} is indeed a representative value for the interstitial gas velocity in the trickling region.

For the liquid-solid interaction, $\underline{F}_{\ell s}^t$, we postulate a form similar to Eq. 8:

$$\underline{F}_{\ell s}^t = -b^t \underline{u}_{\ell t} \tag{13}$$

where b^t is a proportionality constant. Unfortunately, a satisfactory functional form for b^t is not available, and hence we shall rely on empiricism for the purpose of our analysis, as described later. Such recourse to empiricism does not decrease the value of our analysis as our goal is to understand the nature of two-phase flow fields introduced by the fact that pulses and trickling region coexist, not to develop a universal model for trickling flow.

Let us consider a one-dimensional (vertical) downflow of gas at a velocity u_{gt}^{∞}, and liquid at a velocity $u_{\ell t}^{\infty}$, at a uniform liquid holdup of β_t. Such a situation can be expected in a region that is far away from the pulses. It is straightforward to combine Eqs. 3–8 and 10–13 to obtain

$$\epsilon\beta_t(\rho_\ell - \rho_g)g + a^t u_{gt}^{\infty}/(1 - \beta_t) - b^t u_{\ell t}^{\infty} = 0 \tag{14}$$

If we now further require that the conditions in this region correspond to the onset of pulsing, then either from a stability argument (Ng, 1986) or simply in an empirical fashion (Charpentier and Favier, 1975), we can obtain a constraint between u_{gt}^{∞}, $u_{\ell t}^{\infty}$, and β_t (and of course the physical properties of the fluids and the packing), which for the moment we shall simply represent as

$$C_1(u_{gt}^{\infty}, u_{\ell t}^{\infty}, \beta_t) = 0 \tag{15}$$

The important observation to be made at this point is that in the trickling region of Figure 1, one cannot specify u_{gt}^{∞}, $u_{\ell t}^{\infty}$, and β_t arbitrarily, as once one of these three quantities is chosen, Eqs. 14 and 15 determine the other two.

The empiricism enters in our analysis as follows. We shall employ the well-known and widely tested correlation of Charpentier and Favier (1975) for the trickling-to-pulsing transition; see Appendix A. In the text, we shall simply refer to this correlation as Eq. 15, as one can substitute any other correlation or a theoretical model (e.g., Ng, 1986) for the trickling-to-pulsing transition in the place of the Charpentier and Favier correlation, with little change to the concept behind our modeling approach.

It was alluded to earlier that we shall use an empirical approach to estimate b^t. One of the ways in which this can be done is as follows. We use an empirical correlation for liquid holdup in the trickling region, which can be represented in a general form as

$$C_2(u_{gt}^{\infty}, u_{\ell t}^{\infty}, \beta_t) = 0. \tag{16}$$

Thus for a chosen value of u_{gt}^{∞} (say), we can solve for $u_{\ell t}^{\infty}$ and β_t by solving Eqs. 15 and 16. However, for determining flow fields around a pulse we would like to use Eqs. 3–8 and 10–13, as these equations are physically reasonable and simple to use. If this were to be consistent, then b^t should be so chosen that Eq. 14 is satisfied by the $u_{\ell t}^{\infty}$ and β_t values computed from Eqs. 15 and 16 for the specified value of u_{gt}^{∞}. Accordingly, we shall use Eq. 14 to estimate b^t so that the model for the trickling region is consistent with the employed empirical relations. In our analysis, we have used the empirical correlation of Midoux et al. (1976) for liquid holdup as Eq. 16; see Appendix A. In the text, we shall simply refer to this correlation as Eq. 16, as one can substitute any other correlation for liquid holdup in the trickling region, which is at a state corresponding to the onset of pulsing or a theoretical model for b^t in the place of the Midoux et al. correlation, with little change to the concept behind our modeling approach.

Returning to the scheme depicted in Figure 1, Eqs. 1, 2, 15, and 16 provide four equations to determine the five unknowns shown in this figure. In order to develop the fifth equation, it is necessary to analyze in some detail the flow fields in a pulse and the trickling region surrounding it. Let us first consider a circular liquid pulse of radius R_p in a large two-dimensional packed column. Far away from this pulse, the gas and the liquid are flowing down with velocities u_{gt}^{∞} and $u_{\ell t}^{\infty}$, respectively, at a liquid holdup of β_t. Choosing a stationary frame of reference whose origin is the same as the center of the pulse at the current instant, and r and θ directions as shown in Figure 2, we can write that

$$\underline{u}_{gt} \longrightarrow u_{gt}^{\infty}\cos\theta\underline{e}_r - u_{gt}^{\infty}\sin\theta\underline{e}_\theta \tag{17}$$

$$\underline{u}_{\ell t} \longrightarrow u_{\ell t}^{\infty}\cos\theta\underline{e}_r - u_{\ell t}^{\infty}\sin\theta\underline{e}_\theta \tag{18}$$

as $r \longrightarrow \infty$. The pulse itself will be moving downward at a velocity

$$\underline{v}_p = v_p\cos\theta\underline{e}_r - v_p\sin\theta\underline{e}_\theta \tag{19}$$

where v_p is the speed of the pulse to be determined. We have assumed that all the pulses in the actual column are of equal size and that these pulses are sufficiently far apart that it suffices to consider an isolated pulse. It will be shown later that the fraction of bed volume occupied by the pulses at throughputs commonly encounterd in practice is usually less than 0.1. Therefore treating the pulses as independent of one another is quite reasonable. [By putting forward the above visualization for pulses, we have added an unknown (namely, v_p) to those in Figure 1, so that we have to develop two more equations to complete the fluid mechanical description of the problem.]

The flow fields inside the trickling region are described by Eqs. 3–7, with Eqs. 17 and 18 providing the conditions away from the pulse. If we require that a state of onset of pulsing exist everywhere in the trickling region, then necessarily the liquid holdup will vary as a function of position around the pulse. This would render the analysis very complex. To simplify the analysis, we postulate that the condition of trickling-to-pulsing transi-

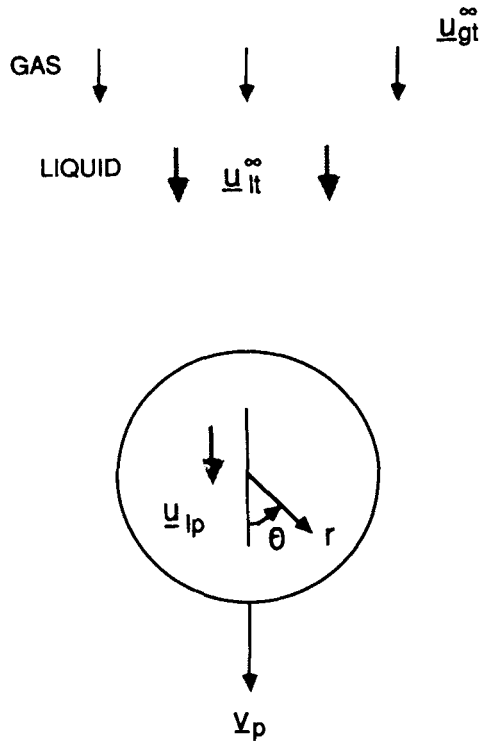

Figure 2. Scheme of gas, liquid, and pulse flows for Eqs. 17–19.

tion—i.e., Eq. 15—exists only in the trickling region far away from the pulse, and relax this requirement in the vicinity of the pulse. Instead we assume that the liquid holdup is uniform everywhere in the trickling region. An immediate consequence of this assumption is that the coefficients a^t and b^t in Eqs. 8 and 13 are constant everywhere in the trickling region, and as a result Eqs. 3–7 become linear.

The volume-averaged continuity and approximate momentum balance equations for the steady flow of liquid inside the pulse are given by

$$\nabla \cdot \underline{u}_{\ell p} = 0 \tag{20}$$

$$\epsilon \rho_\ell \underline{g} - \epsilon \nabla p_{\ell p} + \underline{F}_{\ell s}^{p} = \underline{0} \tag{21}$$

A simple constitutive relation for $\underline{F}_{\ell s}^{p}$ can be readily written as

$$\underline{F}_{\ell s}^{p} = -a^p \underline{u}_{\ell p} \tag{22}$$

The coefficient a^p can be estimated from the Ergun equation to obtain

$$a^p = a_{1p} + a_{2p}|\underline{u}_{\ell p}| \tag{23}$$

where

$$a_{1p} = k_{1p}(1 - \epsilon)^2 \mu / \epsilon d_e^2 \tag{24}$$

$$a_{2p} = k_{2p}(1 - \epsilon)\rho_\ell / d_e \tag{25}$$

At the interface between the pulse and the surrounding trickling region, the jump mass balance for the gas and liquid phases yields

$$\underline{v}_p \cdot \underline{n} = \underline{u}_{gt} \cdot \underline{n} \tag{26}$$

$$(\underline{u}_{\ell p} - \underline{v}_p) \cdot \underline{n} = \beta_t (\underline{u}_{\ell t} - \underline{v}_p) \cdot \underline{n} \tag{27}$$

where $\underline{n}$ is a unit normal at the interface. The jump momentum balance at this interface yields

$$p_{\ell t} - p_{\ell p} + \rho_\ell \beta_t (\underline{u}_{\ell t} \cdot \underline{n} - \underline{v}_p \cdot \underline{n})^2 - \rho_\ell (\underline{u}_{\ell p} \cdot \underline{n} - \underline{v}_p \cdot \underline{n})^2 = 0 \tag{28}$$

In the above equation we have used the pressure in the liquid phase of the trickling region, $p_{\ell t}$, as opposed to using p_{gt} or an average pressure over the liquid and gas phases [say $\beta_t p_{\ell t} + (1 - \beta_t) p_{gt}$]. This is because it appears that $p_{\ell t}$ is the most realistic of the three, since it is the liquid phase that is continuous across this interface. In any case, it turns out that for the present problem the choice of pressure [$p_{\ell t}$, p_{gt}, or $\beta_t p_{\ell t} + (1 - \beta_t) p_{gt}$] does not have any effect on the final outcome.

In order to determine the velocity profiles in the trickling region and inside the pulse, we should now solve Eqs. 3–7, 20, 21, and 26–28. If we postulate that the motion of the gas phase can be treated as irrotational, then an explicit, analytical solution can be obtained as described below. We assume that

$$\underline{u}_{gt} = -\nabla \phi_{gt} \tag{29}$$

It then follows that

$$\phi_{gt} = -u_{gt}^{\infty} r \left[1 + \frac{R_p^2 (1 - v_p / u_{gt}^{\infty})}{r^2}\right] \cos\theta \tag{30}$$

and

$$p_{gt} = P_{gt}^{o} + \rho_g g r \cos\theta + a^t \phi_{gt} / \epsilon (1 - \beta_t) \tag{31}$$

where P_{gt}^{o} is an undetermined constant. Recall that we have assumed that β_t is uniform everywhere in the trickling region and that H_t depends only on β_t. It then follows that $p_{\ell t}$ differs from p_{gt} by a constant value (equal to the capillary pressure) everywhere in the trickling region. Therefore we can write that

$$p_{\ell t} = P_{\ell t}^{o} + \rho_g g r \cos\theta + a^t \phi_{gt} / \epsilon (1 - \beta_t) \tag{32}$$

It then follows that

$$\underline{u}_{\ell t} = \frac{1}{b^t}\left[\epsilon \beta_t (\rho_\ell - \rho_g)\underline{g} + \frac{a^t \underline{u}_{gt}}{(1 - \beta_t)}\right] \tag{33}$$

It is then straightforward to show from Eqs. 20 and 27 that

$$\underline{u}_{\ell p} = u_{\ell p}^{o} \cos\theta \underline{e}_r - u_{\ell p}^{o} \sin\theta \underline{e}_\theta \tag{34}$$

where

$$u_{\ell p}^{o} = v_p [1 - \beta_t + \beta_t a^t / b^t (1 - \beta_t)] + \epsilon \beta_t^2 (\rho_\ell - \rho_g) g / b^t \tag{35}$$

Equation 34 implies that inside the pulse, the liquid is moving vertically downward. It readily follows from Eq. 21 that

$$p_{\ell p} = P^o_{\ell p} + \left(\rho_\ell g - \frac{a^p u^o_{\ell p}}{\epsilon}\right) r \cos\theta \qquad (36)$$

where $P^o_{\ell p}$ is an undetermined constant, which needs to be related to $P^o_{\ell t}$ by applying the jump momentum balance at the pulse interface. When Eqs. 32–36 are substituted into Eq. 28 it becomes readily apparent that the jump momentum balance cannot be satisfied exactly everywhere on the pulse surface. This is not surprising as our assumption of a circular pulse is hardly realistic. [Similar difficulty is encountered in the analysis of bubble motion in fluidized beds (Jackson, 1971).] As the assumption of a sharp interface between the pulse and the trickling region is realistic only at the front of the pulse, a reasonable scheme to adopt is to require that the jump momentum balance be satisfied exactly at the nose of the pulse (i.e., $r = R_p$, $\theta = 0$) and try to satisfy as many terms as possible in the Taylor series expansion of the jump momentum balance in terms of θ around the point ($r = R_p$, $\theta = 0$). [This is identical to the approach employed in the analysis of bubble motion in fluidized beds (Jackson, 1971).] The details of this analysis are presented in Appendix B. It follows from this analysis that

$$(\rho_\ell - \rho_g)g + \frac{a^t u^\infty_{gt}}{\epsilon(1-\beta_t)}\left[1 + f^*\left(1 - \frac{v_p}{u^\infty_{gt}}\right)\right] - \frac{a^p u^\infty_{\ell p}}{\epsilon} - F_H \rho_\ell \frac{(1-\beta_t)}{\beta_t}(u^o_{\ell p} - v_p)^2 = 0 \qquad (37)$$

where $f^* = 1$ and $F_H = 2/R_p$. Equations 35 and 37 are the two equations we sought to develop. Equations 1, 2, 15, 16, 35, and 37 should be solved to determine the five unknowns in Figure 1 (namely, f_p, $u^\infty_{\ell t}$, u^∞_{gt}, β_t, and $u^o_{\ell p}$) and v_p. In order to solve these equations we need to specify the throughputs G and L, physical properties of the fluids and packing, various constants in the Ergun equation and correlations employed, and the pulse radius.

It is instructive to examine the various terms in Eq. 37. The first term is the net gravitational force. The second term is the form drag exerted on the pulse by the surrounding trickling region. The third term is the resistance experienced by the liquid inside the pulse as a result of the packing solid. The last term is the force required to accelerate the slowly moving fluid in the trickling region ahead of the pulse to the velocity of the liquid inside the pulse. Each of these terms has been expressed per unit volume of the liquid inside the pulse. Note that as the pulse radius increases, the acceleration term becomes less significant. This results in an increase in the pulse velocity as the size of the pulse increases. Computational results show, however, that for $R_p > \sim 2$ cm, the effect of pulse size on the pulse velocity is insignificant. Noting that the pulses in trickle beds are considerably larger in size, we conclude that the acceleration (i.e., inertial) term in Eq. 37 is insignificant for pulse sizes of practical interest.

The analysis described above for the two-dimensional packed column can readily be modified for the case of a three-dimensional column with spherical pulses. Without presenting the details, we simply note that the final model Eqs. 1, 2, 14–16, 35, and 37 are still valid, except that the quantity f^* in Eq. 37 is equal to 0.5 for the three-dimensional case, while it was equal to unity for the two-dimensional case.

Computations were carried out for the air-water system; the results are summarized in Figures 3 and 4. The results shown there are obtained for a pulse radius of 0.1 m, although increasing the pulse radius has little effect on the results. The parameter values used in the model calculations are presented in Table 1. Figure 3 shows how the average liquid holdup in the bed, defined as $\bar{\beta} = \beta_t(1 - f_p) + f_p$; the liquid holdup in the trickling region, β_t; the fraction of bed volume occupied by the pulses, f_p; and the pulse velocity, v_p, vary with liquid throughput for a fixed gas throughput. When the liquid throughput is increased, $\bar{\beta}$ increases while β_t decreases by a small amount. Also shown for comparison are some experimental data on average liquid holdup measured by Christensen (1986) in a two-dimensional column. It must be noted that the uncertainty associated with

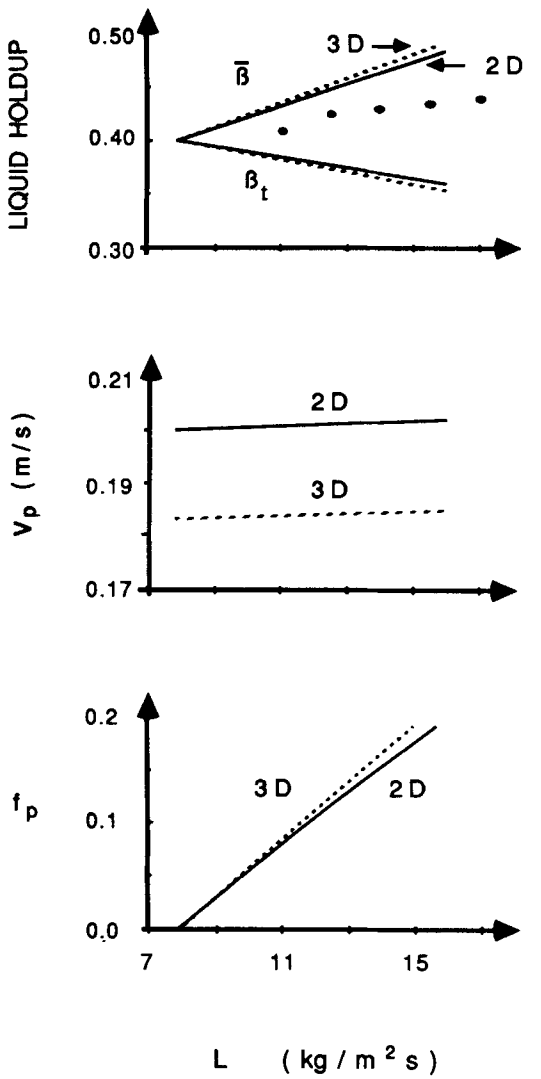

Figure 3. Average liquid holdup in bed and liquid holdup in trickling region (top), pulse velocity (middle), fraction of bed volume occupied by pulses (bottom), all vs. liquid (water) throughput.

Gas (air) throughput, $G = 0.4$ kg/m^2 · s; $R_p = 0.1$ m
2-D column with circular pulses; 3-D column with sperical pulses
●●● average liquid holdup measured by Christensen (1986).

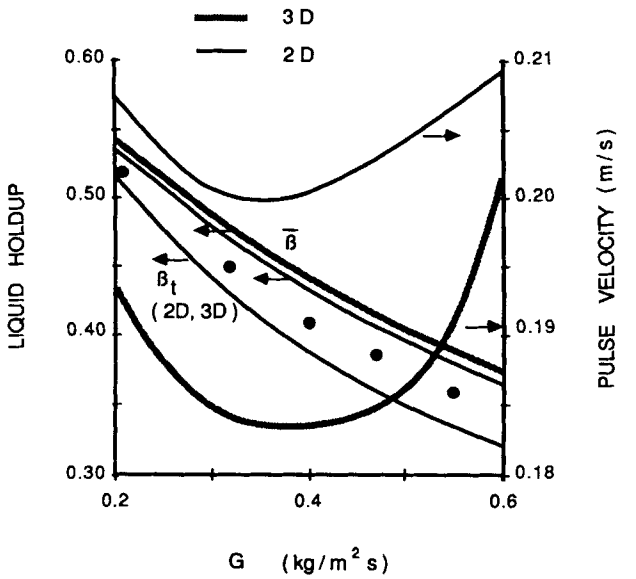

Figure 4. Average liquid holdup in bed, liquid holdup in trickling region, and pulse velocity vs. gas (air) throughput.

Liquid (water) throughput, $L = 11$ kg/m^2 · s; $R_p = 0.1$ m
●●● average liquid holdup measured by Christensen (1986).

the microwave technique used by Christensen for holdup measurement is quite substantial and that within the range of experimental accuracy it was concluded by him that the average liquid holdup is hardly dependent on the liquid flow rate. Drinkenburg and coworkers also arrived at this conclusion from their holdup estimates using conductivity measurements (Blok and Drinkenburg, 1982; Blok et al., 1983; Rao and Drinkenburg, 1983). It is clear from Figure 3 that the model predicts a more appreciable variation of liquid holdup with liquid throughput than is observed experimentally.

It can be seen from Figure 3 that as L increases, the fraction of bed volume occupied by the pulses increases, as one would expect. The pulse velocity is virtually independent of liquid throughput and this trend is quite consistent with the experimental observations (Blok and Drinkenburg, 1983; Blok et al., 1983; Rao and Drinkenburg, 1983; Christensen, 1986). It readily follows from the fact that f_p increases as L increases while v_p is independent of L, that the frequency of pulses increases as L increases (assuming that the pulse size remains constant), which is qualitatively consistent with the experimental observations of Blok and Drinkenburg (1982), Blok et al. (1983), and Rao and Drinkenburg (1983).

The pulse velocities predicted by the model are appreciably smaller than the values measured experimentally. It is clear from Figure 3 that the pulse velocity in a three-dimensional (3-D) column is smaller than that in a two-dimensional (2-D) column, according to the model. This can be traced to the fact that f^* (3-D) is smaller than f^* (2-D) and consequently the form drag exerted by the trickling region on the pulse is smaller in a 3-D column than in a 2-D column. It is interesting to note that the pulse velocities measured in a 2-D column (Christensen et al., 1986) were generally lower than those reported in the literature for small-diameter cylindrical columns. The analysis described above illustrates that this difference cannot be attributed to the change in the geometry from 3-D to 2-D. This leaves the bypassing of gas around pulses, which was more easily accomplished in the two-dimensional column of large width but not in the small-diameter cylindrical columns, as the most likely explanation for the lower pulse velocities measured by Christensen et al. (1986).

Table 1. Parameter Values Used in the Simulations

$d_e = 0.003$ m	$\epsilon = 0.37$
$\rho_w = \rho_\ell = 1{,}000$ kg/m^3	$\rho_g = 1.3$ kg/m^3
$\mu_w = \mu = 0.001$ kg/m · s	$g = 1.4 \times 10^{-5}$ kg/m · s
$k_{1t} = 94$	$k_{1p} = 150$
$k_{2t} = 1.6$	$k_{2p} = 1.75$
$g = 9.8$ m/s^2	$\sigma_\ell = \sigma_w$

Figure 4 shows the variation of $\bar{\beta}$, β_t, and v_p with gas throughput at a constant liquid throughput. Also shown for comparison are some experimental data on average liquid holdup measured by Christensen (1986) in a two-dimensional column. The experimental $\bar{\beta}$ values are somewhat lower than the model predictions, although well within experimental error. The value of β_t steadily declines as G increases, and this is also qualitatively consistent with the trend reported by Blok and Drinkenburg (1982), Blok et al. (1983), and Rao and Drinkenburg (1983).

The model predicts that the pulse velocity is a very weak function of G and this is inconsistent with the experimental results, which indicate a very strong dependence of v_p on G. We are thus faced with two major questions:

- Why does the model predict pulse velocities that are much smaller than experimental data?
- Why does the model not predict the strong dependence of v_p on G observed experimentally?

An inspection of the model assumptions and the resulting equations suggests two possibilities.

1. The assumption that the pulse contains only liquid is a possible reason for the low values of v_p. This can be illustrated as follows. If we allow the pulse to contain gas, then an approximate expression for the pulse velocity is

$$v_p \simeq (\beta_p u^o_{\ell p} - \beta_t u^\infty_{\ell t})/(\beta_p - \beta_t) \tag{38}$$

where β_p is the fraction of void volume inside the pulse occupied by liquid. The model, and heuristically the very existence of pulses, indicate that $u^o_{\ell p} > u^\infty_{\ell t}$. It is clear from Eq. 38 that for fixed values of $u^o_{\ell p}$, $u^\infty_{\ell t}$, and β_t, as we decrease β_p from 1.0 the value of v_p increases. However, the increase in v_p obtained by decreasing β_p is usually quite small until β_p becomes very close to β_t (in eq. 38). As the experimental results indicate that β_p is appreciably larger than β_t (Rao and Drinkenburg, 1983), it appears unlikely that neglecting the presence of gas bubbles in the pulse is the primary reason for the inconsistencies between the model and the experiments.

2. The lack of sensitivity of v_p on G indicates that the model grossly underestimates the form drag exerted by the trickling region on the pulse. In fact, an analysis of the various terms in Eq. 37 indicates that the form drag term in Eq. 37 is only a small fraction of the net gravitational force term. Thus, according to the model, the liquid in the pulse is for the most part simply falling under its own weight. Therefore, we have to explore possible modifications that would increase the contribution of the form drag term in Eq. 37. This is equivalent to investigating how the value of f^* in Eq. 37 can be made larger, i.e., more realistic.

Note that in the limit $f^* \to \infty$, $v_p \to u_{gt}^{\infty}$, and this indeed is the upper limit for pulse velocities observed experimentally.

In this paper we explore reasons why f^* may be larger than the value of 1.0 predicted by the above analysis for two-dimensional columns. We focus our attention on such columns because of the mathematical simplicity associated with this geometry. Although the presence of gas bubbles inside the pulse could be quite significant, including this in the analysis is not possible at the present time, as suitable momentum balance equations for the gas and liquid phases inside the pulse are far from obvious.

Before we proceed any further, it is useful to present the gas and liquid streamlines in and around the pulse. It readily follows from Eqs. 30, 33, and 34 that the velocity potentials $\hat{\phi}$ for the gas and liquid in a two-dimensional column with respect to a pulse-stationary frame of reference (where origin coincides with the center of the pulse at all times) are given by

$$\begin{aligned}
\hat{\phi}_{gt} &= -(u_{gt}^{\infty} - v_p)(1 + R_p^2/r^2)r\cos\theta + \text{constant} \\
\hat{\phi}_{\ell t} &= S_1 r\cos\theta - S_2 R_p^2\cos\theta/r + \text{constant} \\
\hat{\phi}_{\ell p} &= -(u_{\ell p}^{o} - v_p)r\cos\theta + \text{constant}
\end{aligned} \tag{39}$$

where

$$\begin{aligned}
S_1 &= v_p - \epsilon\beta_t(\rho_\ell - \rho_g)g/b' - a' u_{gt}^{\infty}/(1 - \beta_t)b' \\
S_2 &= a' u_{gt}^{\infty}[1 + f^*(1 - v_p/u_{gt}^{\infty})]/(1 - \beta_t)b'
\end{aligned}$$

Defining stream functions $\hat{\psi}$ such that

$$\frac{\partial\hat{\phi}_j}{\partial r} = \frac{1}{r}\frac{\partial\hat{\psi}_j}{\partial\theta} \quad \text{and} \quad \frac{1}{r}\frac{\partial\hat{\phi}_j}{\partial\theta} = -\frac{\partial\hat{\psi}_j}{\partial\theta}, \qquad j = gt, \ell t, \ell p,$$

one obtains

$$\begin{aligned}
\hat{\psi}_{gt} &= -(u_{gt}^{\infty} - v_p)(1 - R_p^2/r^2)r\sin\theta + \text{constant} \\
\hat{\psi}_{\ell t} &= S_1 r\sin\theta + S_2 R_p^2\sin\theta/r + \text{constant} \\
\hat{\psi}_{\ell p} &= -(u_{\ell p}^{o} - v_p)r\sin\theta + \text{constant}.
\end{aligned} \tag{40}$$

Figure 5 shows the gas and liquid streamlines for a typical set of conditions. The liquid streamlines are almost vertical in the trickling region, and exactly vertical in the pulse. In the pulse-stationary frame of reference, the liquid is moving upward while the gas is flowing downward. In a column of large width, there is ample room for the gas to bypass the pulse. It appears reasonable to expect that any factor that would make it more difficult for the gas to bypass the pulse would increase the form drag exerted by the trickling region on the pulse and, as a result, would speed up the pulse motion. The most obvious factor that one can consider is the possible significance of the fact that the width of the column used by Christensen et al. (1986) (or equivalently the diameter of the cylindrical column) is finite.

Before we present an analysis of the effect of the finite column width, we note that one can combine Eqs. 39 and 40 and define a complex potential $\hat{W}_{gt}$ as

$$\hat{W}_{gt} = \hat{\phi}_{gt} + i\hat{\psi}_{gt} = -(u_{gt}^{\infty} - v_p)(z + R_p^2/z) + \text{constant} \tag{41}$$

where $z = r\cos\theta + ir\sin\theta$, and $i = \sqrt{-1}$. If we use a cartesian coordinate system in the pulse-stationary frame of reference

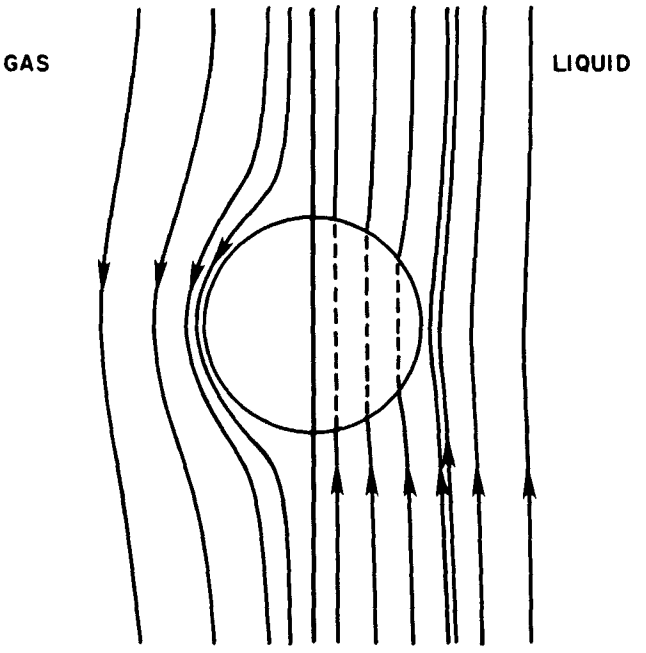

Figure 5. Typical gas and liquid streamlines in a pulse-stationary frame of reference for a circular pulse moving down through a packed column.

with the x axis pointing vertically downwards and the y axis horizontally, we have $z = x + iy$.

Effect of Walls

Let us now consider the motion of a liquid pulse in a two-dimensional column of width $2R_w$. The locations of the walls are given by $y = \pm R_w$. Our approach to treating the effect of the finite column width is an adaptation of the analysis of Collins (1965a,b) for the motion of gas bubbles in a liquid and in a fluidized bed of finite width. Briefly, this treatment recognizes that the complex potential for the flow of gas around a pulse in a column of finite width is equivalent to the complex potential for the flow of gas around an array of identical pulses placed at a distance $2R_w$ apart along the y axis in a column of infinite width. Although this observation by itself does not directly lead to the desired complex potential, an explicit expression for the desired potential can indeed be readily obtained if we can relax our assumption that the pulses are circular. The details of the mathematical treatment can be found in a paper by Collins (1965b). We simply note that a complex potential $\hat{W}_{gt}$ given by

$$\hat{W}_{gt} = \hat{\phi}_{gt} + i\hat{\psi}_{gt} = -(u_{gt}^{\infty} - v_p)\left[z + \frac{R_w\alpha}{\pi}\coth\left(\frac{\pi z}{2R}\right)\right] \tag{42}$$

where

$$\alpha = \frac{\pi R_p}{R_w}\tan\left(\frac{\pi R_p}{2R_w}\right), \tag{43}$$

describes the velocity potential $\hat{\phi}_{gt}$ and stream function $\hat{\psi}_{gt}$ for the flow of gas in the trickling region around a pulse whose

shape is described by

$$y = \left(\frac{R_w \alpha}{\pi}\right)\left\{\sin\left(\frac{\pi y}{R_w}\right)\Big/\left[\cosh\left(\frac{\pi x}{R_w}\right) - \cos\left(\frac{\pi y}{R_w}\right)\right]\right\}. \quad (44)$$

According to Eq. 44, the surface of the pulse intersects the y axis at $\pm R_p$ and the x axis at the locations given by the solutions of

$$\sinh\left(\frac{\pi x}{2R_w}\right) = \pm\sqrt{\frac{\alpha}{2}}. \quad (45)$$

Figure 6 illustrates the pulse shapes for various R_p/R_w values. It is readily apparent that according to the model the pulse elongates as (R_p/R_w) increases. Once the velocity potential for the gas phase is determined from equation 43, it is straightforward to obtain the liquid phase velocity profiles and the pressure profiles in the trickling region and inside the pulse. The application of the jump momentum balance is carried out around the nose of the liquid pulse in a manner analogous to that described in Appendix B for circular pulses. Without presenting the details, we simply note that Eqs. 14–16, 33–35, and 37 remain unchanged except that the quantities f^* and F_H in Eq. 37 are now given by

$$f^* = (3 + 2\alpha)/(3 + \alpha) \quad (46)$$

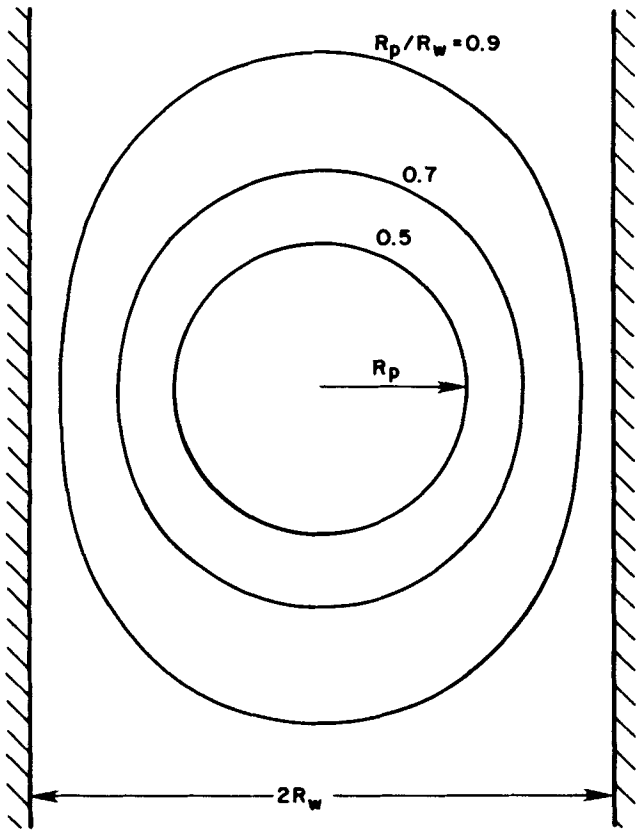

Figure 6. Pulse shapes for different R_p/R_w values, as described by Eq. 44.

and

$$F_H = \left(\frac{2\pi}{R_w}\right)\left(1 + \frac{\alpha}{3}\right)\Big/\sinh\left(\frac{\pi x_L}{R_w}\right) \quad (47)$$

where x_L is the location of the nose of the pulse obtained by solving Eq. 45.

As in the case of circular pulses in a bed of infinite width discussed in the previous section, it was found that the inertial term in Eq. 37 was insignificant for realistically large pulses even when the walls are included. Thus the effect of the walls on the pulse velocity is manifested primarily through Eq. 46. As R_p/R_w increases, the value of α increases unboundedly and this results in the doubling of f^* [from 1 for $R_p \sim o(R_w)$ to 2 for $R_p \sim R_w$]. Such an increase in f^* will indeed increase the value of v_p, as one would expect.

Computations were carried out with the crossflow model [Eqs. 1, 2, 14–16, 35, 37, 46, and 47 for different R_p/R_w values. The resulting pulse velocities for various R_p/R_w values for a typical throughput of gas (air) and liquid (water) are shown in Table 2. It is clear that although the pulse velocity increases with increasing R_p/R_w, this increase is only small. The experimentally observed pulse velocities are typically three to four times larger in magnitude than those in Table 2.

We therefore conclude that the model described above in the section on pulse motion is missing some important pulse characteristic(s) and that the wall effect is only of secondary importance.

Effect of Pulse Shape

In the analysis described in the pulse motion section we assumed that the pulses are circular in shape. In reality, this is far from accurate. Visual observation of pulses in a two-dimensional column indicates that when the pulses do not span the column width they are curved concavely downward (Christensen et al., 1986). Although the front of the pulse could be approximately treated as an arc of a circle, the wake region itself is not too far behind the front of the pulse. Noting that in our analysis we neglect the wake region, a better representation of the pulse would view it as a circular cap in two-dimensional columns and a spherical cap in three-dimensional columns. The reasons for discussing the case of a circular pulse previously are twofold:

1. The analysis described there serves to illustrate the inadequacy of treating the pulse as circular.
2. It is necessary to derive the complex potential for gas flow in the trickling region around a circular pulse, i.e., Eq. 41, before this potential can be suitably modified for a circular cap pulse, as described below.

Our approach to treating the motion of a circular cap pulse is an adaptation to the present problem of the analysis of Collins (1965b) for the motion of dented gas bubbles in fluidized beds.

Returning to the irrotational flow of a gas past a circular pulse in a two-dimensional column of infinite width, it was seen

Table 2. Effect of Wall on Pulse Velocity

R_p/R_w	0.3	0.5	0.8	0.9	0.95
v_p, m/s	0.210	0.211	0.222	0.226	0.228

$G = 0.4$ kg/m^2 · s; $L = 11$ kg/m^2 · s

earlier that the complex potential for the gas flow in a pulse-stationary frame of reference was given by Eq. 41 and the pulse shape itself was defined by

$$|z| = R_p \tag{48}$$

where $z = x + iy$. Let us subject this pulse shape to a conformal mapping described by

$$t = z + R_p d - R_p(1 - d)^2/(z + R_p d) \tag{49}$$

where d is a shape parameter $0 < d \leq 1$ and $t = X + iY$ is a complex variable in the new space. If $d = 1$, then this transformation amounts to simple shifting of the origin as $X = x + R_p$ and $Y = y$. When d is not equal to 1, the shape of the pulse is altered by this mapping. Figure 7 shows the pulse shapes obtained for various values of d and fixed R_p. The shape shown in this figure for small value of d ($d = 0.1$) is indeed very similar to the pulse shapes observed visually in two-dimensional columns (Christensen et al., 1986). (This mapping does not preserve the area of the pulse and hence, strictly speaking, d not only affects the shape but also the size.)

One can rewrite Eq. 49 as

$$z = [t - 2R_p d + \sqrt{t^2 + 4R_p^2(1 - d)^2}]/2 \tag{50}$$

This can be substituted in Eq. 41 to obtain $\hat{W}_{gt}$ in terms of t, and the real and imaginary components can then be separated to obtain $\hat{\phi}_{gt}(X, Y)$ and $\hat{\psi}_{gt}(X, Y)$. It is not difficult to show that the resulting $\hat{\phi}_{gt}(X, Y)$ satisfies the Laplace equation. Thus $\hat{\phi}_{gt}(X, Y)$ does indeed describe the velocity potential of gas flow in this transformed space. It can also be shown that $\hat{\psi}_{gt}(X, Y)$ describes the streamlines for gas flow in the transformed space. With this knowledge of the gas phase flow field, one can readily obtain the liquid phase flow fields in the trickling region and in the pulse. The jump momentum balance is subsequently applied around the nose of the liquid pulse in a manner analogous to that described in Appendix B for circular pulses. Without presenting the details, we simply note that Eqs. 14–16, 35, and 37 remain unchanged except that the quantities f^* and F_H in Eq. 37 are now given by

$$f^* = (1 + 3d^2)/d(3 + d^2) \tag{51}$$

$$F_H = \frac{d(1 + d)(3 + d^2)}{(1 + d^2)^2 R_p} \tag{52}$$

It is interesting to note from Eq. 51 that as d decreases toward zero, f^* increases unboundedly. This in turn results in a monotonic increase in the pulse velocity, with v_p approaching u_{gt}^{∞} as d decreases toward zero. This is illustrated in Table 3 where the pulse velocities computed from the model (i.e., Eqs. 1, 2, 14–16, 35, 37, 51, and 52) for different values of d at a typical operating condition are presented.

It is readily apparent from Eq. 52 that the significance of the inertial term in Eq. 37 should decrease with decreasing d. Our model calculations did not reveal any noticeable effect of R_p on v_p (for $R_p > \sim 2$ cm) for any value of d ($0 < d \leq 1$). Thus we conclude that the dependence of the pulse velocity on the pulse geometry is characterized in our model solely by the shape parameter, d.

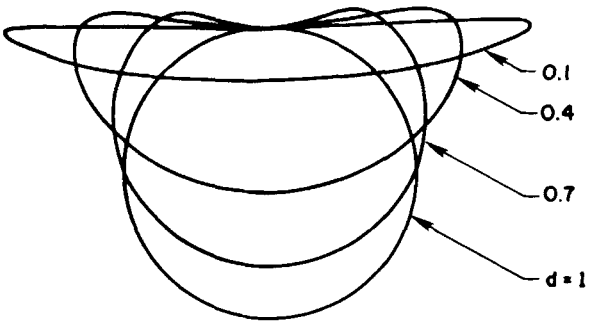

Figure 7. Pulse shapes for different values of d, as described by Eqs. 48 and 49.
Value of R_p held constant

The experimental observation that the pulses in two-dimensional columns are approximately circular-cap in shape (Christensen et al., 1986) and the model result that it is necessary to incorporate the circular-cap shape of a pulse in order to predict pulse velocities comparable to those measured experimentally, strongly suggest that the shape of the pulse is an important parameter in any model for pulsing flow.

The variations of $\bar{\beta}$ and v_p with gas flow rate, as predicted by the model for different values of the pulse shape parameter d, are presented in Figure 8. The pulse velocity is very sensitive to the value of d when d is close to zero. In the limit $d \to 0$, v_p approaches u_{gt}^{∞}, and this limit is also shown in Figure 8. Also shown for comparison are some experimental pulse velocity and liquid holdup data reported by Christensen (1986). The pulse velocity data could, in principle, be fitted to the model for a value of $d = 0.005$.

The average liquid holdup in the bed decreases slightly as d decreases. However, $\bar{\beta}$ is much less sensitive than v_p to a change in d. Under the conditions described in this figure, the fraction of bed volume occupied by the pulses is invariably small (typi-

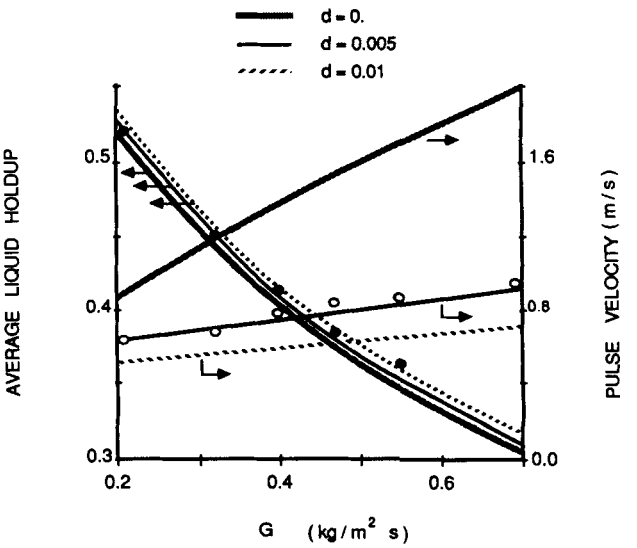

Figure 8. Average liquid holdup in bed and pulse velocity vs. gas (air) throughput for various values of pulse shape parameter d.
Liquid (water) throughput $L = 11$ kg/m² · s.
● average liquid holdups, O pulse velocities measured by Christensen (1986).

Table 3. Effect of Pulse Shape on Pulse Velocity

d	1.0	0.2	0.1	0.01	0.005	0
v_p, m/s	0.210	0.226	0.266	0.596	0.75	1.35

$G = 0.4$ kg/m$^2 \cdot$ s; $L = 11$ kg/m$^2 \cdot$ s
Experimental pulse velocity $\simeq 0.78$ m/s (Christensen, 1986)

cally less than 0.05). As a result, the values of β_t are only slightly smaller than those of $\bar{\beta}$.

Figure 9 shows the variations of $\bar{\beta}$, f_p, and v_p with liquid flow rate for different values of d. The pulse velocity is virtually independent of the liquid flow rate, quite consistent with the experimental trend (Rao and Drinkenburg, 1983). The fraction of bed volume occupied by the pulses increases as L increases, and this results in an increase of $\bar{\beta}$ with L. The variation of $\bar{\beta}$ with L predicted by the model for $d = 0.005$ (which seemed optimal for fitting the v_p data) is somewhat smaller than that observed experimentally by Christensen (1986), although within the experimental accuracy. It is seen in Figure 9 that as d decreases, the value of f_p decreases. This can be readily attributed to an increase in v_p associated with a decrease in d.

The apparent agreement between the model predictions for a very small value of the pulse shape parameter and the experimental results should not be taken too seriously for the following reason. A very small value of d implies that the pulse is essentially a very thin strip of liquid, as is evident from Figure 7. As d decreases, the thickness of the pulse decreases. The ratio between the thickness of the pulse and its width can be shown to be approximately equal to d. Then, if we consider a pulse of 0.3 m width, in order to fit the velocity data the model requires the thickness of this pulse to be approximately equal to 1.5 mm. This of course does not make practical sense as the actual thickness of the pulses is indeed much larger than this value. A value of d smaller than 0.1 is difficult to accept as realistic. It is clear from Table 3 that only a small enhancement in the pulse velocity is realized in the model by decreasing d from 1.0 to 0.1. Thus we are forced to conclude that the model described here is still missing some important characteristics of the pulsing flow. The analysis described in this paper does serve a useful purpose. The inadequacy of the model can be traced to the fact that the model underestimates the drag exerted by the trickling region on the pulses. Our analysis has revealed that although incorporating the presence of confining walls and the circular-cap shape of the pulse will increase this drag, these factors by themselves cannot provide a satisfactory representation of the pulsing flow.

We can make certain speculations as to what important characteristics of pulsing flow are missing in the model. Figure 10 shows the typical gas and liquid streamline for a circular cap pulse predicted by the model used in our study. The gas phase streamlines are appreciably curved around the pulse. When flow past such a bluff object is encountered, one can expect vortices to develop in the gas phase ahead of (i.e., below) the pulse. It was hoped at the outset that the presence of a solid packing would inhibit these vortices from becoming significant, so that

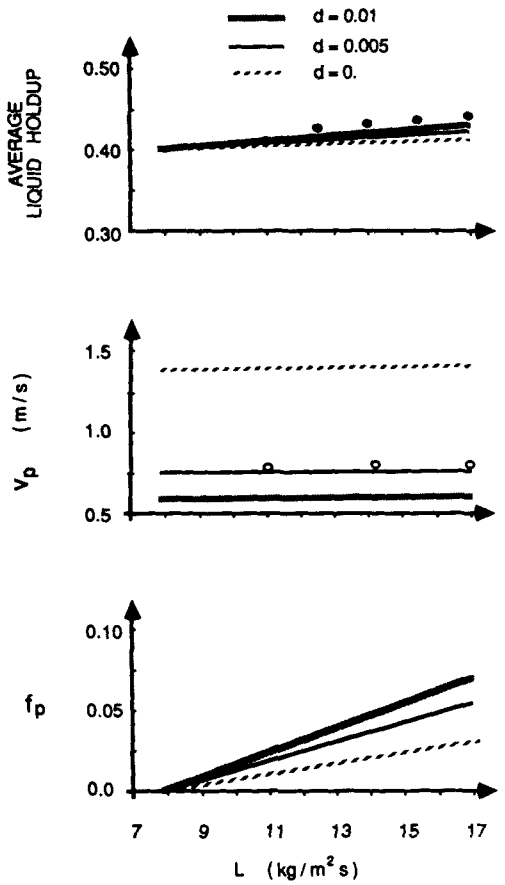

Figure 9. Average liquid holdup in bed (top), pulse velocity (middle), fraction of bed volume occupied by pulses (bottom), all vs. liquid (water) throughput for various values of pulse shape parameter d.

●●● average liquid holdup, O O O pulse velocities, measured by Christensen (1986).

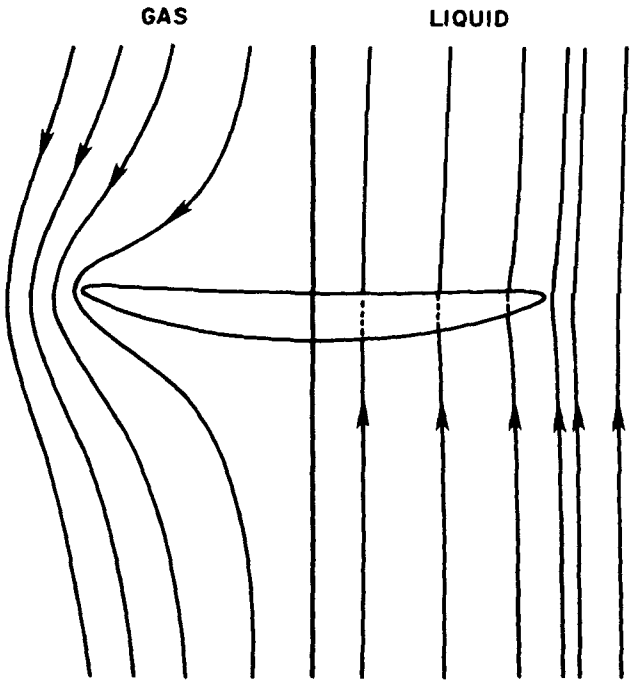

Figure 10. Typical gas and liquid streamlines in a pulse-stationary frame of reference for a circular-cap pulse moving down through a packed column.

an irrotational flow of the gas could be a good first approximation. Apparently this is not so. Future analysis should attempt to include the effects of these gas phase vortices and assert whether the existence of these vortices can indeed lead to a value of about 67 for f^* in Eq. 37 (for realistic pulse shapes), which seems to be necessary to fit the pulse velocity data.

Within the framework of the crossflow model, it can easily be shown that a good estimate of the average pressure gradient, $\langle \nabla P \rangle$, is given by

$$\langle \nabla P \rangle = \frac{1}{\epsilon} [b' u_{\ell t}^{\infty} (1 - f_p) + f_p a^p u_{\ell p}^{o}] - \bar{\beta} \rho_{\ell} g \qquad (53)$$

since $\rho_{\ell} \gg \rho_g$ and the inertial term in Eq. 37 is negligible. Let us assume for the sake of illustration that a value of 67 is obtained for f^* by curve-fitting the pulse velocity data; see Figure 8. Using this value for f^*, the crossflow model Eqs. 1, 2, 14–16, 35, and 37 were solved and the average pressure gradient was estimated for a variety of operating conditions. The results are summarized in Figure 11 along with the experimental data of Christensen (1986). The model predicts that $\langle \nabla P \rangle$ increases almost linearly with the liquid flow rate. This is quite consistent with the experimental trend. The literature correlations for $\langle \nabla P \rangle$ were found by Christensen et al. (1986) to grossly overestimate the actual $\langle \nabla P \rangle$ measured when the pulses do not span the column cross section. The predictions of the model reported here are very close to the actual $\langle \nabla P \rangle$ data. This is remarkable when one takes into consideration the fact that the experimental $\langle \nabla P \rangle$ data under pulsing flow conditions were never used in the estimation of model parameters. The only parameters in the model, k_{1t} and k_{2t}, were determined (Christensen, 1986) by measuring pressure gradient for gas flow over a wetted packing, as recommended by Specchia and Baldi (1977). Although the model slighty underestimates the variation of $\langle \nabla P \rangle$ with gas throughput, by a slight adjustment of the parameters k_{1t} and k_{2t} the model can be made to reproduce the data quite nicely. We will not indulge in such a retrofitting exercise, as the purpose of the above discussion is to illustrate that the modeling approach described in this paper is leading us in the right direction.

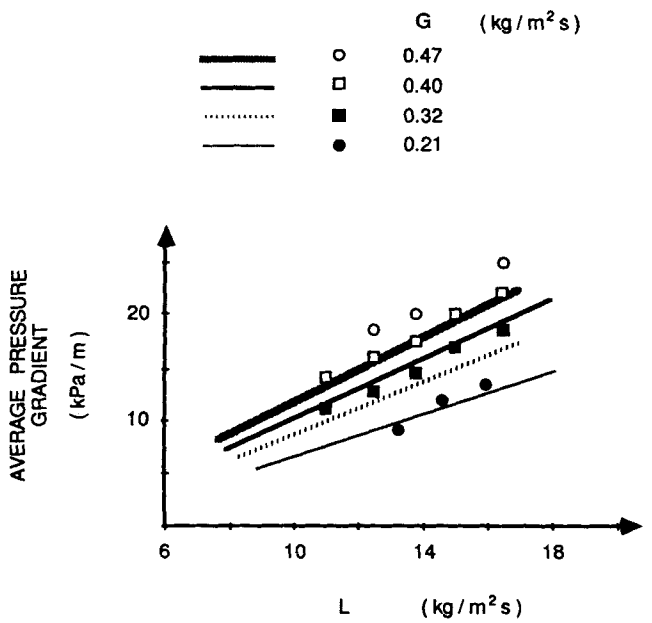

Figure 11. Average pressure gradient vs. liquid (water) flow rate for various gas (air) flow rates.

Let us return briefly to our discussion of modifying the model to account for the gas phase vortices. It can be seen in Figure 10 that the liquid streamlines are virtually vertical even though the gas streamlines are appreciably curved around the pulse. This suggests that in a volume-averaged analysis the liquid streamlines may continue to remain virtually vertical even if we include gas phase vortices. If this is true, then no dramatic enhancement in the lateral mixing in the liquid phase should be observed when the operating conditions are shifted from trickling regime to pulsing regime in a trickle bed of large cross section. In contrast, an appreciable increase should be observed in the gas phase lateral mixing upon moving to pulsing regime from trickling regime (as the existence of pulses increases the tortuosity for the gas flow). An experimental study of lateral dispersion in the gas and liquid phase in a large trickle bed could therefore provide a qualitative guideline in formulating an improved model for pulsing flow. For example, if the liquid streamlines are indeed almost vertical, then it may be argued that the only significant way in which the gas phase vortices would affect the model equations is through the term f^* in Eq. 37.

Although the assumption of a sharp increase in the liquid holdup (from that of the trickling region to that in the pulse) at the front of a pulse is experimentally supportable, the model assumption of a sharp decrease in liquid holdup at the back of a pulse could be a significant factor in the failure of the model. However, relaxing this assumption renders the problem almost intractable.

Liquid Exchange between Pulse and Trickling Region

In order that a crossflow model of the type discussed in the previous sections be useful in analyzing performance characteristics such as axial dispersion in the liquid phase, mass transfer, and the like, it is necessary to develop expressions for the rate at which liquid is exchanged between the pulse and the trickling region. The detailed analysis of the flow fields in and around a pulse permits the development of an expression for this exchange rate. As an illustration, consider the case of circular pulses of radius R_p in a two-dimensional packed column discussed in the pulse-motion model section. It is straightforward to show that the rate of liquid exchange between the pulses and the trickling region per unit volume of bed in this case is equal to $2\epsilon f_p \rho_{\ell} (v_p - u_{\ell p}^{o})/\pi R_p$. Thus, even though the pulse radius was not important in determining the pulse velocity, it is important in determining the rate of liquid exchange between the pulse and the trickling region. Even though the irrotational flow model described in the previous sections is deficient, it is instructive to consider some typical values for the exchange rate of liquid. In the context of circular pulses, the time required to flush out the liquid in a pulse can easily be shown to be equal to $\pi R_p / 2(v_p - u_{\ell p}^{o})$. Since $(v_p - u_{\ell p}^{o}) \simeq \beta_t (v_p - u_{\ell t}^{\infty})$ and $v_p \gg u_{\ell t}^{\infty}$, the flushing time is approximately equal to $\pi R_p / 2\beta_t v_p$. Thus the distance traveled by the pulse before being completely flushed out is approximately equal to $\pi R_p / 2\beta_t$. Using a conservative value of 0.25 for β_t, we see that a pulse is flushed out completely by the time it travels a distance of about six times its radius. Considering that the trickle beds used commercially are very tall, it

appears reasonably certain that the pulse will get flushed out several times before it exits the column.

Summary

By dividing the trickle bed into two regions, namely the pulses and the trickling flow region surrounding these pulses, a simple crossflow model has been formulated. For simplicity the pulses were assumed to be made up of only liquid, and the gas flow around the pulses was assumed to be irrotational. The resulting irrotational flow model underestimates the pulse velocity substantially when the pulses are assumed to be circular in a two-dimensional column or, equivalently, spherical in a three-dimensional column. Although incorporating the presence of confining walls and the circular-cap shape of the pulses can increase the pulse velocities predicted by the model somewhat, this procedure cannot eliminate the inconsistencies between the model and the data. It is suspected that the effects of the vortices in the gas phase ahead of the pulses and/or the wake region behind the pulses should be incorporated into the model before the model can become predictive.

Notation

a^p = proportionality constant, Eq. 22, defined by Eq. 23
a^t = proportionality constant, Eq. 8, defined by Eq. 12
a_{1p}, a_{2p} = see Eqs. 23–25
a_{1t}, a_{2t} = see Eqs. 10–12
b^t = proportionality constant, Eq. 13
d = pulse shape parameter, Eq. 49
d_e = effective diameter of packing particles
$\underline{e}_r, \underline{e}_\theta$ = unit vectors
f^* = quantity in term characterizing form drag exerted by trickling region on pulse, Eq. 37
f_p = fraction of bed volume occupied by pulses
F_H = quantity resembling curvature in acceleration term, Eq. 37
$\underline{F}^p_{\ell s}, \underline{F}^t_{\ell s}$ = drag force per unit bed volume exerted by solid on liquid in pulse and trickling region, Eqs. 13, 22
$\underline{F}^t_{\ell g}$ = drag force per unit bed volume exerted by gas and gas-liquid interface on liquid in trickling region, Eq. 7
$\underline{F}^t_{g\ell}$ = drag force per unit bed volume exerted by liquid and gas-liquid interface on gas in trickling region, Eqs. 7, 8
$g, \underline{g}$ = acceleration due to gravity
G = gas throughput, kg/m^2 · s
H_t = average curvature of gas-liquid interface at any location in the bed, Eq. 6
k_{1p}, k_{2p} = Ergun constants in pulse, Eqs. 24, 25
k_{1t}, k_{2t} = Ergun constants in trickling region, Eqs. 10, 11
L = liquid throughput, kg/m^2 · s
$\underline{M}^t$ = interaction force arising from local fluctuations in curvature of gas-liquid interface (Drew, 1983), Eq. 7
$\underline{n}$ = unit normal at interface between pulse and trickling region
$p_{\ell p}$ = pressure in liquid in pulse
$p_{gt}, p_{\ell t}$ = pressures in gas and liquid phases in trickling region
$\langle \nabla P \rangle$ = average pressure gradient
r = radial coordinate
R_p = pulse radius
R_w = half-distance between walls
S_1, S_2 = quantities for velocity potential and stream function for liquid in trickling region; See expressions after Eqs. 39, 40
t = complex variable $X + iY$
$u^\infty_{gt}, u^\infty_{\ell t}$ = average velocities of gas and liquid in trickling region with respect to a stationary frame of reference
$\underline{u}_{gt}, \underline{u}_{\ell t}$ = velocities of gas and liquid in trickling region with respect to a stationary frame of reference
$u^a_{\ell p}$ = average velocity of liquid in pulse with respect to a stationary frame of reference
$\underline{u}_{\ell p}$ = velocity of liquid in pulse with respect to a stationary frame of reference
v_p = pulse velocity
$\hat{W}_{gt}$ = complex potential for gas in trickling region, Eqs. 41, 42
x, X = vertical coordinates
x_L = location of nose of pulse obtained by solving Eq. 45
y, Y = horizontal coordinates
z = complex variable $x + iy$

Greek letters

α = quantity, Eq. 43
β_t, β_p = liquid holdup (fraction of void volume occupied by liquid) in trickling region and pulse
$\bar{\beta}$ = average liquid holdup in bed
ϵ = porosity of bed
ρ_g, ρ_ℓ = densities of gas and liquid
σ = gas-liquid interfacial tension
μ_g, μ_ℓ = viscosities of gas and liquid
$\phi_{gt}, \hat{\phi}_{gt}$ = velocity potential for the gas in the trickling region with respect to a stationary and a pulse-stationary frame of reference
$\hat{\phi}_{\ell t}, \hat{\phi}_{\ell p}$ = velocity potentials for liquid in trickling region and in pulse with respect to a pulse-stationary frame of reference
$\hat{\psi}_{gt}, \hat{\psi}_{\ell t}, \hat{\psi}_{\ell p}$ = stream functions for gas in trickling region, liquid in trickling region, and liquid in pulse with respect to a pulse-stationary frame of reference

Appendix A

In our analysis we have employed an empirical approach to describe Eqs. 15 and 16 in the text. The well-known correlation for trickling-to-pulsing transition proposed by Charpentier and Favier (1975) can be rewritten as

$$u^\infty_{\ell t} - \frac{1{,}000 u^\infty_{gt}\rho_g(1-\beta_t)}{\rho_\ell \beta_t \lambda \psi}\left[\frac{10\epsilon\rho_g(1-\beta_t)u^\infty_{gt}}{\lambda}\right]^{-1.17} = 0 \quad \text{(A1)}$$

where

$$\lambda = (\rho_g\rho_\ell/\rho_w\rho_{air})^{1/2}$$

$$\psi = (\sigma_w/\sigma_\ell)[(\mu_\ell/\mu_w)(\rho_w/\rho_\ell)^2]^{1/3}$$

Here σ_w is the interfacial tension of the air-water interface; ρ_{air} and ρ_w are the densities of air and water, respectively; μ_w is the viscosity of water. We have used Eq. A1 in place of Eq. 15 in the text.

The correlation of Midoux et al. (1976) was found by Christensen et al. (1986) to be quite satisfactory for describing the average liquid holdup in the two-dimensional column under pulsing flow conditions for the air-water system. Hence it appears reasonable to hope that the liquid holdup at the conditions corresponding to the trickling-to-pulsing transition will be satisfactorily modeled by this correlation. According to this correlation,

$$\beta_t - 0.66\chi^{0.81}/(1 + 0.66\chi^{0.81}) = 0 \quad \text{(A2)}$$

where

$$\chi = (\delta_\ell/\delta_g)^{1/2}$$

$$\delta_g = \frac{150\mu_g(1-\epsilon)^2}{d_e^2\epsilon^2}[u^\infty_{gt}(1-\beta_t)] + \frac{1.75(1-\epsilon)\rho_g}{d_e\epsilon}[u^\infty_{gt}(1-\beta_t)]^2$$

$$\delta_\ell = \frac{150\mu_\ell(1-\epsilon)^2}{d_e^2\epsilon^2}(u^\infty_{\ell t}\beta_t) + \frac{1.75(1-\epsilon)\rho_\ell}{d_e\epsilon}(u^\infty_{\ell t}\beta_t)^2$$

We have used Eq. A2 in place of Eq. 16 in the text. It must be emphasized that we have used this correlation only for estimating the holdup in the trickling region, not for determining the average liquid holdup in the column.

Appendix B

It follows from Eqs. 26 and 33 that at $r = R_p$,

$$\underline{u}_{\ell t} \cdot \underline{n} = u^o_{\ell t} \cos\theta$$

where

$$u^o_{\ell t} = \frac{1}{b'}\left[\epsilon\beta_t(\rho_\ell - \rho_g)g + a^t v_p/(1-\beta_t)\right] \tag{B1}$$

and $\underline{n} = \underline{e}_r$ is a unit vector in the radial direction. Introduce the above result, and Eqs. 27, 32, 34, and 36 into Eq. 28 to obtain

$$\begin{aligned} P^o_{\ell t} - P^o_{\ell p} - (\rho_\ell - \rho_g)gR_p\cos\theta \\ + (a^p u^o_{\ell p}/\epsilon)R_p\cos\theta - a^t u^\infty_{gt}R_p\delta\cos\theta \\ + \rho_\ell\beta_t(u^o_{\ell t} - v_p)^2\cos^2\theta - \rho_\ell(u^o_{\ell p} - v_p)^2\cos^2\theta = 0 \end{aligned} \tag{B2}$$

where

$$\delta = 2 - v_p/u^\infty_{gt}.$$

If we require that Eq. B2 be satisfied exactly at $\theta = 0$, we obtain

$$\begin{aligned} P^o_{\ell t} - P^o_{\ell p} - (\rho_\ell - \rho_g)gR_p + (a^p u^o_{\ell p}/\epsilon)R_p \\ - a^t u^\infty_{gt}R_p\delta + \rho_\ell\beta_t(u^o_{\ell t} - v_p)^2 - \rho_\ell(u^o_{\ell p} - v_p)^2 = 0 \end{aligned} \tag{B3}$$

Subtracting Eq. B3 from Eq. B2 to eliminate $P^o_{\ell t}$ and $P^o_{\ell p}$,

$$\begin{aligned} F(\theta) \equiv (\rho_\ell - \rho_g)R_p(1-\cos\theta) + a^t u^\infty_{gt}R_p\delta(1-\cos\theta) \\ - (a^p u^o_{\ell p}/\epsilon)R_p(1-\cos\theta) + \rho_\ell(u^o_{\ell p} - v_p)^2(1-\cos^2\theta) \\ - \rho_\ell\beta_t(u^o_{\ell t} - v_p)^2(1-\cos^2\theta) = 0 \end{aligned} \tag{B4}$$

Clearly, this cannot be satisfied for every θ, $0 \le \theta \le \pi$. We demand that this equation be satisfied in the vicinity of $\theta = 0$. Differentiating $F(\theta)$ with respect to θ,

$$\begin{aligned} \frac{dF}{d\theta} = (\rho_\ell - \rho_g)R_p\sin\theta + a^t u^\infty_{gt}R_p\delta\sin\theta - (a^p u^o_{\ell p}/\epsilon)R_p\sin\theta \\ + 2\rho_\ell(u^o_{\ell p} - v_p)^2\sin\theta\cos\theta - 2\rho_\ell\beta_t(u^o_{\ell t} - v_p)^2\sin\theta\cos\theta = 0 \end{aligned} \tag{B5}$$

Equation B5 if automatically satisfied at $\theta = 0$. Differentiating one more time with respect to θ,

$$\begin{aligned} \frac{d^2F}{d\theta^2} = (\rho_\ell - \rho_g)R_p\cos\theta + a^t u^\infty_{gt}R_p\delta\cos\theta - (a^p u^o_{\ell p}/\epsilon)R_p\cos\theta \\ + 2\rho_\ell(u^o_{\ell p} - v_p)^2(\cos^2\theta - \sin^2\theta) \\ - 2\rho_\ell(u^o_{\ell t} - v_p)^2\beta_t(\cos^2\theta - \sin^2\theta) = 0 \end{aligned} \tag{B6}$$

The desired jump momentum balance, Eq. 37, is obtained by requiring that Eq. B6 be satisfied exactly at $\theta = 0$, followed by a minor algebraic manipulation involving the introduction of Eq. 27.

Literature cited

Beimesch, W. E., and D. P. Kessler, "Liquid-Gas Distribution Measurements in the Pulsing Regime of Two-Phase Cocurrent Flow in Packed Beds," *AIChE J.*, **17,** 1160 (1971).

Blok, J. R., and A. A. H. Drinkenburg, "Hydrodynamic Properties of Pulses in Two-Phase Downflow-Operated Packed Columns," *Chem. Eng. J.*, **25,** 89 (1982).

Blok, J. R., J. Varkevisser, and A. A. H. Drinkenburg, "Transition to Pulsing Flow, Holdup and Pressure Drop in Packed Columns with Cocurrent Gas-Liquid Downflow," *Chem. Eng. Sci.*, **38,** 687 (1983).

Charpentier, J. C., and M. Favier, "Some Liquid Holdup Experimental Data in Trickle Bed Reactors for Foaming and Nonfoaming Hydrocarbons," *AIChE J.*, **21,** 1213 (1975).

Christensen, G., "Hydrodynamics of Two-Dimensional Trickle Beds," M.S. Thesis, Princeton Univ. (1986).

Christensen, G., S. J. McGovern, and S. Sundaresan, "Cocurrent Downflow of Air and Water in a Two-Dimensional Packed Column," *AIChE J.*, **32,** 1677 (1986).

Collins, R., "A Simple Model of the Plane Gas Bubble in a Finite Liquid," *J. Fluid Mech.*, **22,** 763 (1965a).

———, "An Extension of Davidson's Theory of Bubbles in Fluidized Beds," *Chem. Eng. Sci.*, **20,** 747 (1965b).

Davidson, J. F., "Symposium on Fluidization—Discussion," *Trans. Inst. Chem. Eng.*, **39,** 230 (1961).

Davidson, J. F., and D. Harrison, *Fluidization,* Academic Press, London and New York (1971).

Dimenstein, D. M., and K. M. Ng, "A Model for Pulsing Flow in Cocurrent Downflow Trickle Bed Reactors," *Chem. Eng. Commun.*, **41,** 215 (1986).

Drew, D. A., "Mathematical Modelling of Two-Phase Flow," *Ann. Rev. Fluid Mech.*, **15,** 261 (1983).

Gianetto, A., G. Baldi, V. Specchia, and S. Sicardi, "Hydrodynamics and Solid-Liquid Contacting Effectiveness in Trickle-Bed Reactors," *AIChE J.*, **24,** 1087 (1978).

Herskowitz, M., and J. M. Smith, "Trickle-Bed Reactors: A Review," *AIChE J.*, **29,** 1 (1983).

Hoffman, H., "Multiphase Catalytic Packed-Bed Reactors," *Catal. Rev. Sci. Eng.*, **17,** 21 (1978).

Jackson, R., "Fluid Mechanical Theory of Fluidization," *Fluidization,* J. F. Davidson and D. Harrison, eds., Academic Press, London and New York (1971).

Koros, R. M., "Scale-up Considerations for Mixed-Phase Catalytic Reactors," *Multiphase Chemical Reactors. II: Design Methods,* A. E. Rodriguez, J. M. Calo, and N. H. Sweed, eds., Sijthoff and Noordhoff (1981).

Lerou, J. J., D. Glasser, and D. Luss, "Packed-Bed Liquid Phase Dispersion in Pulsed Gas-Liquid Downflow," *Ind. Eng. Chem. Fundam.*, **9,** 66 (1980).

McGovern, S. J., "Pulsing Flow Hydrodynamics and Mass Transfer," second proposition submitted to Chem. Eng. Dept., Princeton Univ. (1982).

Midoux, N., M. Favier, and J. C. Charpentier, "Flow Pattern, Pressure Loss and Liquid Holdup Data in Gas-Liquid Downflow through Packed Beds with Foaming and Nonfoaming Hydrocarbons," *J. Chem. Eng. Japan,* **9,** 350 (1976).

Ng, K. M., "A Model for Flow Regime Transitions in Cocurrent Downflow Trickle-Bed Reactors," *AIChE J.*, **32,** 115 (1986).

Rao, V. G., and A. A. H. Drinkenburg, "Pressure Drop and Hydrodynamic Properties of Pulses in Two-Phase Gas-Liquid Downflow through Packed Columns," *Can. Chem. Eng. J.*, **62,** 158 (1983).

Saéz, A. E. and R. G. Carbonell, "Hydrodynamic Parameters for Gas-Liquid Cocurrent Flow in Packed Beds," *AIChE J.*, **31,** 52 (1985).

Sato, Y., T. Hirose, F. Takahashi, and M. Toda, "Pressure Loss and Liquid Holdup in Packed-Bed Reactor with Cocurrent Gas-Liquid Downflow," *J. Chem. Eng. Japan,* **6,** 147 (1973).

Satterfield, C. N., "Trickle-Bed Reactors," *AIChE J.*, **21,** 209 (1975).
Shah, Y. T., *Gas-Liquid-Solid Reactor Design,* McGraw-Hill, New York (1979).
Specchia, V., and G. Baldi, "Pressure Drop and Liquid Holdup for Two-Phase Concurrent Flow in Packed Beds," *Chem. Eng. Sci.*, **32,** 515 (1977).
Tosun, G., "A Study of Cocurrent Downflow for Nonfoaming Gas-Liquid Systems in a Packed Bed. 2: Pressure Drop—Search for a Correlation," *Ind. Eng. Chem. Process Des. Dev.*, **23,** 35 (1984).
Weekman, V. W., Jr., and J. E. Myers, "Fluid Flow Characteristics of Cocurrent Gas-Liquid Flow in Packed Beds," *AIChE J.*, **10,** 951 (1964).

Manuscript received May 16, 1986, and revision received Sept. 8, 1986.